J Geodesy (2007) 81:121–136
DOI 10.1007/s00190-006-0094-0

ORIGINAL ARTICLE

A comparison of the tesseroid, prism and point-mass approaches for mass reductions in gravity field modelling

B. Heck · K. Seitz

Received: 2 March 2006 / Accepted: 16 August 2006 / Published online: 26 September 2006

Abstract The calculation of topographic (and isostatic) reductions is one of the most time-consuming operations in gravity field modelling. For this calculation, the topographic surface of the Earth is often divided with respect to geographical or map-grid lines, and the topographic heights are averaged over the respective grid elements. The bodies bounded by surfaces of constant (ellipsoidal) heights and geographical grid lines are denoted as tesseroids. Usually these ellipsoidal (or spherical) tesseroids are replaced by "equivalent" vertical rectangular prisms of the same mass. This approximation is motivated by the fact that the volume integrals for the calculation of the potential and its derivatives can be exactly solved for rectangular prisms, but not for the tesseroids. In this paper, an approximate solution of the spherical tesseroid integrals is provided based on series expansions including third-order terms. By choosing the geometrical centre of the tesseroid as the Taylor expansion point, the number of non-vanishing series terms can be greatly reduced. The zero-order term is equivalent to the point-mass formula. Test computations show the high numerical efficiency of the tesseroid method versus the prism approach, both regarding computation time and accuracy. Since the approximation errors due to the truncation of the Taylor series decrease very quickly with increasing distance of the tesseroid from the computation point, only the elements in the direct vicinity of the computation point have to be separately evaluated, e.g. by the prism formulas. The results are also compared with the point-mass formula. Further potential refinements of the tesseroid approach, such as considering ellipsoidal tesseroids, are indicated.

Keywords Topographic reduction · Newton's integral · Tesseroid · Prism method · Point-mass modelling

B. Heck (✉) · K. Seitz
Geodetic Institute, University of Karlsruhe, Englerstraße 7, 76128 Karlsruhe, Germany
e-mail: heck@gik.uni-karlsruhe.de

K. Seitz
e-mail: seitz@gik.uni-karlsruhe.de

1 Introduction

Modelling the effect of mass distributions on gravity-field-related quantities is one of the central issues in physical geodesy. In the classical Stokes's theory of geoid determination (e.g. Heiskanen and Moritz 1967), the effect of the topographic masses above the geoid, as well as the isostatic balance masses on gravity observed on the Earth's surface, has to be calculated. Besides this topographic–isostatic reduction of gravity, the indirect effect on the gravitational potential has to be considered for a proper determination of the geoid, which is a surface situated inside the Earth's masses below the continents.

Even in the theory of Molodensky et al. (1962), although originally free of any mass reductions (e.g. Moritz 1980), the terrain reduction enters as a correction term G_1 in the first-order solution of Molodensky's series. In many modern local and regional gravity field modelling concepts, the residual terrain modelling (RTM) approach is often applied in the framework of the remove-compute-restore (RCR) technique for smoothing the gravity field (Forsberg and Tscherning 1997); here, the masses between the Earth's surface and a

smoothed boundary surface have to be taken into account for both in the remove and in the restore step.

Although the basic analytical formulas for the calculation of mass effects on gravity and on the gravitational potential look very simple, a precise evaluation is very time-consuming due to the irregular structure of the surfaces bounding the masses (e.g. Earth's topographic surface). Computation time is still an issue nowadays when high-resolution digital terrain models (DTMs) with a resolution of up to 30" (e.g. Rodriguez et al. 2005) – potentially in connection with digital density models – are used, since volume integrals have to be solved that, in principle, extend over the whole globe in horizontal extension.

In geodesy and geophysics, many procedures for an efficient calculation of the topographical mass effects have been proposed and adapted to the computational tools available at those times. The traditional procedure of splitting the topographic masses into a Bouguer plate and the residual terrain (Heiskanen and Vening Meinesz 1958) exactly serves this purpose: the major part of the topographic reduction, attributed to an infinite planar Bouguer plate or spherical shell of constant density, can be calculated very easily. On the other hand, the terrain reduction is generally smaller, except in mountainous areas, and the integration can be restricted to the neighbourhood of the computation point due to the strong decrease of the topographical effect with increasing distance; often the terrain reduction has been completely neglected in geophysical prospecting applications.

Since an infinite planar Bouguer plate approximates the shape of the topography very poorly, many authors advocate the use of a more realistic spherical Bouguer shell (e.g. Smith et al. 2001; Vaníček et al. 2001, 2004; LaFehr 1991a); the relationship between the planar and the spherical Bouguer corrections was discussed, e.g. by LaFehr (1991b) and Hackney and Featherstone (2003).

In order to get simple computation formulas for the terrain reduction, the terrain can also be subdivided into concentric circles and their radii related to the computation point (Hammer 1939; Heiskanen and Moritz 1967, p 130; Nowell 1999). The calculation of the terrain reduction using concentric circle templates, also known as Hammer charts, is very time-consuming due to the fact that for each computation point, the process of estimating mean elevations over the surface elements bounded by circles and horizontal radii has to be started anew. This procedure was widely used in the pre-computer era (Jung 1961) and has been replaced by another approach based on DTMs provided in files of different grid size. The respective topographic cells in a DTM are bounded either by geographic or planar (e.g. UTM) grid lines.

Assuming a constant topographic height and mass-density in each cell, the resulting bodies are often approximated by rectangular prisms having the same volume as the original columns over the cells. It is an advantage of the rectangular prisms that the respective volume integrals for calculating the effects on gravity and potential can be solved analytically – although the evaluation of these formulas requires the numerical calculation of several logarithmic and arctan functions (Mader 1951; Nagy 1966; Forsberg 1984; Tsoulis 1999; Nagy et al. 2000, 2002). Furthermore, the prisms are inclined with respect to the local vertical and shifted with respect to the horizontal plane at the computation point, due to the (approximate) sphericity of the Earth. These effects have to be taken into account for distant prismatic elements (Grüninger 1990; Kuhn 2000; Smith 2000, 2002).

In the vicinity of the computation point, the flat-topped prism is only a rough approximation of the topographic surface, resulting in discontinuities in the DTM surface. A better approximation is provided by a prism topped by an inclined plane (Koch 1965; Grüninger 1990) or by a bilinear surface (Smith 2000; Smith et al. 2001; Tsoulis et al. 2003). The approach based on these inclined-top prisms can be easily extended to general polyhedral bodies (Talwani and Ewing 1960; Paul 1974; Petrović 1996; Tsoulis 1999; Tsoulis et al. 2003), applying Gauß's divergence theorem; this procedure requires the numerical calculation of a 1D line integral, which can efficiently be solved by numerical methods.

Considering the gravity-field-related quantities of geodetic interest, the integration over the vertical coordinate in the respective volume integrals can be performed analytically, if a constant or laterally-varying topographic density is postulated. In this way, 2D integrals over the infinite plane or a spherical reference surface have to be evaluated numerically (Martinec 1998; Novák et al. 2001; Heck 2003a; Vaníček et al. 2004) since the integral kernels are rather complicated.

The effect of distant masses in terms of surface or volume integrals is often approximated by series expansions of the respective integral kernels, neglecting, e.g. second and higher order terms. This principle is the basis of the widely used terrain correction C of gravity expressed as a planar or spherical integral of the type (e.g. Moritz 1968; Forsberg 1984; Forsberg and Sideris 1989, and many subsequent papers)

$$C = \frac{1}{2} G\rho \iint_S \frac{\left(H' - H_p\right)^2}{\ell_o^3} \mathrm{d}S \tag{1}$$

where H' and H_p are the topographic heights of the integration and computation points, respectively, separated

by the horizontal distance ℓ_o; G is Newton's constant of gravitation, ρ the (constant) mass density, and dS the surface element of the (planar or spherical) reference surface S.

The linear approximation given by Eq. (1) is the first term of a series expansion converging for $\left|(H' - H_p)/\ell_o\right| < 1$, i.e. for terrain slopes less than 45° (e.g. Martinec et al. 1996; Jekeli and Serpas 2003). The integral in Eq. (1) in the planar case can be expressed as convolutions of H' and $(H')^2$, allowing the application of 2D FFT techniques (Forsberg 1984, 1985; Sideris 1985; Harrison and Dickinson 1989; Schwarz et al. 1990; Klose and Ilk 1993; Li and Sideris 1994).

As an alternative, Eq. (1) – understood as a spherical integral – can be calculated by a 1D convolution in longitude (Smith 2002). In order to overcome the difficulties with the aforementioned convergence criterion in rough terrain, Tsoulis (1999) and Tsoulis and Tziavos (2002) have proposed a combination of space- and frequency-domain techniques.

In this contribution, an alternative space-domain approach to the calculation of topographic–isostatic reductions is presented, which is based on series expansions of the kernel functions related to the gravitational effects of so-called *tesseroids*; these elementary bodies result from a subdivision of the ellipsoidal or spherical reference surface into elements bounded by geographical grid lines and have a constant (ellipsoidal or spherical) height. The proposed procedure (cf. Seitz and Heck 2001) can be understood as an extension of MacMillan's idea (MacMillan 1930; Anderson 1976) to spherical or ellipsoidal tesseroids, while MacMillan's original formulas – related to rectangular prisms – refer to the planar approximation of topographic or terrain reduction.

In Sect. 2, the prism method for mass reductions in gravity field modelling is reviewed, and the series expansion by MacMillan is derived in our terminology. In Sect. 3, an analogous procedure is applied to the gravitational field of a spherical tesseroid. Both sets of formulas are compared with respect to precision and computing time in Sect. 4, while Sect. 5 concludes with some proposals for further extensions.

2 Review of the prism potential

The gravitational potential u of a right rectangular parallelopiped (prism) of homogeneous mass-density ρ is described by Newton's integral

$$u(x,y,z) = G\rho \int_{z_1}^{z_2}\int_{y_1}^{y_2}\int_{x_1}^{x_2} \frac{\mathrm{d}x'\mathrm{d}y'\mathrm{d}z'}{\ell} \tag{2}$$

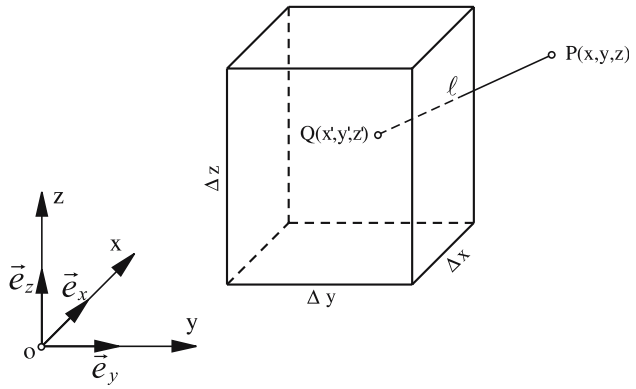

Fig. 1 Geometry of the rectangular prism

where

$$\ell = \sqrt{(x-x')^2 + (y-y')^2 + (z-z')^2} \tag{3}$$

denotes the Euclidean distance between the computation point $P(x,y,z)$ and the running integration point $Q(x',y',z')$. The coordinate axes in Eq. (2) have been assumed to be parallel to the edges of the prism, which extends between the coordinate surfaces related to the bounds $x_1, x_2, y_1, y_2, z_1, z_2$ (Fig. 1).

It is well known that the integral in Eq. (2) can be solved analytically (Mader 1951; Grüninger 1990; Nagy et al. 2000, 2002), resulting in the formula for the potential $u(x, y, z)$

$$\begin{aligned} u(x,y,z) &= G\rho \sum_{i=1}^{2}\sum_{j=1}^{2}\sum_{k=1}^{2} (-1)^{i+j+k} \\ &\times \Bigg[(x-x_i)(y-y_j)\ln\left|\frac{z-z_k+w_{ijk}}{\sqrt{(x-x_i)^2+(y-y_j)^2}}\right| \\ &+ (y-y_j)(z-z_k)\ln\left|\frac{x-x_i+w_{ijk}}{\sqrt{(y-y_j)^2+(z-z_k)^2}}\right| \\ &+ (z-z_k)(x-x_i)\ln\left|\frac{y-y_j+w_{ijk}}{\sqrt{(z-z_k)^2+(x-x_i)^2}}\right| \\ &- \frac{1}{2}\Bigg((x-x_i)^2 \arctan\frac{(y-y_j)(z-z_k)}{(x-x_i)w_{ijk}} \\ &+ \left(y-y_j\right)^2 \arctan\frac{(z-z_k)(x-x_i)}{(y-y_j)w_{ijk}} \\ &+ (z-z_k)^2 \arctan\frac{(x-x_i)(y-y_j)}{(z-z_k)w_{ijk}} \Bigg) \Bigg], \end{aligned} \tag{4}$$

with $w_{ijk} = \sqrt{(x-x_i)^2 + (y-y_j)^2 + (z-z_k)^2}$.

The logarithmic terms in Eq. (4) have been transformed with respect to Mader's (1951) formula in order to provide a better numerical stability (cf. Grüninger 1990). The direct application of Eq. (4) will fail when the computation point P is situated on an edge or on a corner of the prism; the respective limit values have been derived by Nagy et al. (2000, 2002).

The gradient of the potential

$$\operatorname{grad} u = u_x \vec{e}_x + u_y \vec{e}_y + u_z \vec{e}_z \tag{5}$$

is related to the partial derivatives of u with respect to the Cartesian coordinates x, y, z ($\vec{e}_x, \vec{e}_y, \vec{e}_z$ are the unit vectors in the direction of the coordinate axes), where

$$\begin{aligned} u_x(x,y,z) = G\rho \sum_{i=1}^{2}\sum_{j=1}^{2}\sum_{k=1}^{2} (-1)^{i+j+k} \\ \times \left[(y-y_j) \ln \left| \frac{z - z_k + w_{ijk}}{\sqrt{(x-x_i)^2 + (y-y_j)^2}} \right| \right. \\ + (z-z_k) \ln \left| \frac{y - y_j + w_{ijk}}{\sqrt{(x-x_i)^2 + (z-z_k)^2}} \right| \\ \left. - (x-x_i) \arctan \frac{(y-y_j)(z-z_k)}{(x-x_i) w_{ijk}} \right]. \end{aligned} \tag{6}$$

Again, the logarithmic terms have been modified in order to improve their numerical stability.

Equation (6) can be derived either by differentiating the potential (Eq. (4)) with respect to x or by solving directly the differentiated equation (2)

$$u_x(x,y,z) = -G\rho \int_{z_1}^{z_2}\int_{y_1}^{y_2}\int_{x_1}^{x_2} \frac{(x-x')\,\mathrm{d}x'\mathrm{d}y'\mathrm{d}z'}{\ell^3}. \tag{7}$$

The other two partial derivatives u_y and u_z can be obtained from Eq. (6) by cyclic permutation. Limit values of u_x, u_y and u_z for the case that the computation point is situated on an edge or a corner of the prism, are provided in Nagy et al. (2000, 2002).

Due to the decrease of gravitational effects with increasing distance (Newton's law), the rather complex and time-consuming Eqs. (4) and (6) may be substituted by much simpler expressions based on a Taylor expansion of the integrand in Eq. (2) and subsequent integration. Maximum efficiency can be achieved if the Taylor point is fixed at the geometrical centre of the prism, i.e.

$$\begin{aligned} x_o &= (x_1 + x_2)/2, \\ y_o &= (y_1 + y_2)/2, \\ z_o &= (z_1 + z_2)/2. \end{aligned} \tag{8}$$

Formally, the Taylor expansion of the integral kernel $1/\ell$ can be expressed by

$$\begin{aligned} I = \ell^{-1} &= \left[(x'-x)^2 + (y'-y)^2 + (z'-z)^2 \right]^{-1/2} \\ &= \sum_{i,j,k} \mathrm{I}_{ijk} (x'-x_o)^i (y'-y_o)^j (z'-z_o)^k \end{aligned} \tag{9}$$

where

$$I_{ijk} := \frac{1}{(i+j+k)!} \left. \frac{\partial^{i+j+k} \ell^{-1}}{\partial x'^i \partial y'^j \partial z'^k} \right|_{\substack{x'=x_o \\ y'=y_o \\ z'=z_o}}. \tag{10}$$

Inserting Eq. (9) into Eq. (2), it becomes obvious that the integration with respect to each coordinate can be reduced to integrals of the type

$$\begin{aligned} \int_{x_1}^{x_2} (x'-x_o)^i \mathrm{d}x' &= \int_{-\Delta x/2}^{+\Delta x/2} (x'')^i \mathrm{d}x'' \\ &= \frac{1-(-1)^{i+1}}{(i+1)2^{i+1}} (\Delta x)^{i+1} \\ &= \begin{cases} 0 & \text{if } i \text{ odd} \\ (\Delta x)^{i+1} / \left[(i+1)2^i \right] & \text{if } i \text{ even,} \end{cases} \end{aligned} \tag{11}$$

where $\Delta x = x_2 - x_1$ (and similarly $\Delta y = y_2 - y_1, \Delta z = z_2 - z_1$). As a consequence, only those terms for which i, j and k are even will remain in the resulting series, while all other terms cancel out due to our specific choice of the Taylor point $P_o(x_o, y_o, z_o)$. This procedure is comparable to the classical Gauß mid-latitude formulas for the equations of the geodesic (e.g. Heck 2003b, p. 210), and produces a very fast numerical convergence.

The gravitational potential of the homogeneous rectangular prism, neglecting terms of order four and higher in $\Delta x, \Delta y, \Delta z$, is then given by MacMillan's (1930) formula (also see, Anderson 1976; Forsberg 1984)

$$\begin{aligned} u(x,y,z) = G\rho \Delta x \Delta y \Delta z \\ \times \left[\frac{1}{\ell_o} + \frac{3(x_o - x)^2 - \ell_o^2}{24 \ell_o^5} \Delta x^2 \right. \\ + \frac{3(y_o - y)^2 - \ell_o^2}{24 \ell_o^5} \Delta y^2 \\ \left. + \frac{3(z_o - z)^2 - \ell_o^2}{24 \ell_o^5} \Delta z^2 + O(\Delta^4) \right] \end{aligned} \tag{12}$$

where ℓ_o denotes the Euclidean distance between the computation point P and the geometrical centre P_o of the prism (see Fig. 2):

$$\ell_o = \sqrt{(x_o - x)^2 + (y_o - y)^2 + (z_o - z)^2}.$$

The Landau symbol $O(\Delta^m)$ in Eq. (12) indicates that terms of the order m and higher are neglected.

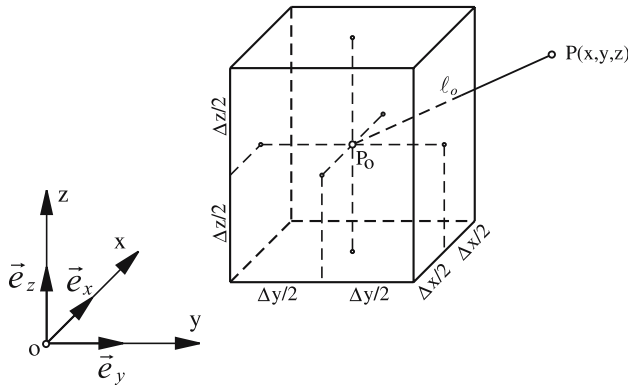

Fig. 2 Geometry of the MacMillan approximation

From Eq. (12) it is obvious that the zero-order approximation is formally identical with the potential of a point-mass at P_o when the total mass of the prism $m = \rho\Delta x\Delta y\Delta z$ is concentrated at its geometrical centre P_o:

$$u(x,y,z) = \frac{G\rho\Delta x\Delta y\Delta z}{\ell_o}[1 + O(\Delta^2)]. \tag{13}$$

The residual terms in Eq. (12) take into account the deviations from a point-mass and vanish for a cube, i.e. when $\Delta x = \Delta y = \Delta z$.

The first and higher order derivatives of the potential can be simply found by differentiation with respect to x, y and z. Numerical investigations concerning the convergence of Eq. (12), as well as a generalization of the MacMillan formulas for the non-homogeneous prism based on a linear density model, have been presented by Anderson (1976). The MacMillan (1930) formula (Eq. 12) and its derivatives have also been implemented in the *TC* software by Forsberg (1984) for prismatic topographic elements situated in an intermediate zone, while the point-mass approximation Eq. (13) is used for large distances, and the exact prism formulas Eqs. (4) and (6) are used for the near zone.

Due to the curvature of the Earth, the topocentric Cartesian coordinate systems, attached to the direction of the vertical at the computation point P – on the one hand – and to the edges of the prismatic topographic element – on the other hand – will not be parallel. Taking into account the convergence of the plumbline directions, the situation is visualized in Fig. 3 where (X, Y, Z) denote the Cartesian coordinates related to a global terrestrial (equatorial) reference frame and (x, y, z) and (x^*, y^*, z^*) the local Cartesian coordinates related to the edge system of the prism and to the local vertical reference frame at the computation point P, respectively.

The transformation of the components u_x, u_y, u_z of the effect on the gravity vector, described in the edge system of the prism, into the local system at P is provided by the respective basis transformations with respect to the global equatorial system. Approximating the direction of the plumbline at the computation point P by the ellipsoidal normal (geodetic latitude φ and longitude λ) and the direction of the z-axis of the edge system by the parameters φ', λ', the relations between the orthonormal base vectors in the respective triads can be expressed by the following formulas (Grüninger 1990; Kuhn 2000)

$$(\vec{e}_x, \vec{e}_y, \vec{e}_z)^{\mathrm{T}} = \mathbf{P}_1 \cdot \mathbf{R}_2\left(\frac{\pi}{2} - \varphi'\right) \cdot \mathbf{R}_3(\lambda') \cdot (\vec{e}_X, \vec{e}_Y, \vec{e}_Z)^{\mathrm{T}} \tag{14a}$$

$$(\vec{e}_x^*, \vec{e}_y^*, \vec{e}_z^*)^{\mathrm{T}} = \mathbf{P}_1 \cdot \mathbf{R}_2\left(\frac{\pi}{2} - \varphi\right) \cdot \mathbf{R}_3(\lambda) \cdot (\vec{e}_X, \vec{e}_Y, \vec{e}_Z)^{\mathrm{T}}. \tag{14b}$$

where $\mathbf{R}_2$ and $\mathbf{R}_3$ denote rotation matrices for rotations about the 2- and 3-axes, respectively, while the reflective matrix $\mathbf{P}_1$ has to be introduced for the transition between the right-handed global terrestrial frame $(\vec{e}_X, \vec{e}_Y, \vec{e}_Z)$ and the left-handed local terrestrial systems $(\vec{e}_x, \vec{e}_y, \vec{e}_z)$ and $(\vec{e}_x^*, \vec{e}_y^*, \vec{e}_z^*)$, oriented to geodetic north, east and up.

From Eq. (14b), the formulas for the transformation between the edge system of the prism and the local vertical system at the computation point P result in

$$(u_x^*, u_y^*, u_z^*)^{\mathrm{T}} = \mathbf{T}(\varphi, \lambda; \varphi', \lambda') \cdot (u_x, u_y, u_z)^{\mathrm{T}} \tag{15}$$

$$\mathbf{T}(\varphi, \lambda; \varphi', \lambda') = \mathbf{P}_1 \cdot \mathbf{R}_2\left(\frac{\pi}{2} - \varphi\right) \cdot \mathbf{R}_3(\lambda - \lambda') \cdot \mathbf{R}_2\left(\varphi' - \frac{\pi}{2}\right) \cdot \mathbf{P}_1, \tag{16}$$

where (u_x, u_y, u_z) and (u_x^*, u_y^*, u_z^*) denote the coordinates of the gravity vector grad u in the edge system and in the local vertical system at P, respectively. The explicit form of the transformation matrix $\mathbf{T}$ can be taken from Kuhn (2000, p. 76) and Heck (2003b, p. 41). This transformation has to be performed for any single prism. In practical applications, the geodetic latitudes φ, φ' may be replaced by the geocentric latitudes.

In general, the dimensions of the prism have to be derived from the dimensions of a tesseroid. In Sect. 4, the relations are evaluated under the postulate of equality of the prism and tesseroid masses.

3 Gravitational potential and attraction by tesseroids

As mentioned in Sect. 1, a tesseroid (this notion was introduced by Anderson 1976) is an elementary body

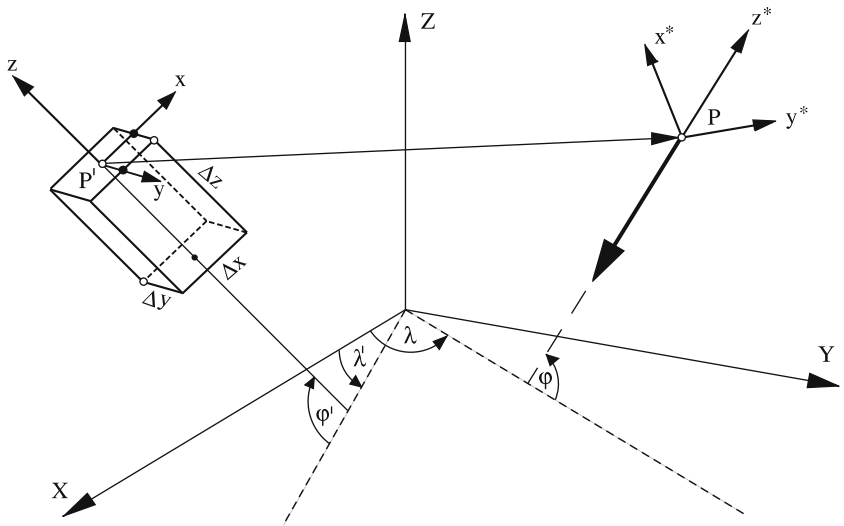

Fig. 3 Transformation between the edge system of the prism and the local vertical reference frame at the computation point P

bounded by geographical grid lines on the ellipsoidal (or spherical) reference surface and surfaces of constant ellipsoidal (or spherical) height. This type of mass elements is created quite naturally when DTMs are used that are based on geodetic coordinates $\varphi,\ \lambda$. The bounding surfaces of a tesseroid are (i) a pair of surfaces of constant ellipsoidal height $h_1 = \text{const}$, $h_2 = \text{const}$, "parallel" to the reference ellipsoid; (ii) a pair of meridional planes $\lambda_1 = \text{const}$, $\lambda_2 = \text{const}$; and (iii) a pair of coaxial circular cones $\varphi_1 = \text{const}$, $\varphi_2 = \text{const}$.

In most cases, a spherical approximation of the ellipsoidal tesseroid will yield sufficient results (Novák and Grafarend 2005). Neglecting the ellipticity of the reference surface the surface pair (i) then consists of concentric spheres with radii $r_1 = R + h_1, r_2 = R + h_2$, where R denotes the chosen radius of the equivalent sphere. The geometrical relations for a spherical tesseroid are visualized in Fig. 4, since the following derivations are restricted to spherical tesseroids.

The gravitational potential v of a spherical tesseroid of homogeneous mass-density ρ is described by Newton's integral

$$v(r,\varphi,\lambda) = G\rho \int_{\lambda_1}^{\lambda_2}\int_{\varphi_1}^{\varphi_2}\int_{r_1}^{r_2} \frac{r'^2 \cos\varphi' \mathrm{d}r' \mathrm{d}\varphi' \mathrm{d}\lambda'}{\ell} \tag{17}$$

where

$$\ell = \sqrt{r^2 + r'^2 - 2rr'\cos\psi} \tag{18}$$

denotes the Euclidean distance between the computation point $P(r,\varphi,\lambda)$ and the running integration point $Q(r',\varphi',\lambda')$ and ψ is the angle between the position vectors of P and Q,

$$\cos\psi = \sin\varphi\sin\varphi' + \cos\varphi\cos\varphi'\cos(\lambda' - \lambda). \tag{19}$$

In contrast to the gravitational potential of the prism Eq. (2) the potential of the tesseroid cannot be solved by elementary integration since elliptic integrals occur. However, an approximate solution can be produced by numerical integration of either the volume integral Eq. (17) or the surface integral resulting from integration over the radial coordinate r'

$$\begin{aligned} v(r,\varphi,\lambda) = \frac{1}{2}G\rho \int_{\lambda_1}^{\lambda_2}\int_{\varphi_1}^{\varphi_2} \cos\varphi' \\ \times\big[\ell\big(r' + 3r\cos\psi\big) + r^2(3\cos^2\psi - 1) \\ \times\ln(\ell + r' - r\cos\psi)\big]\big|_{r'=r_1}^{r'=r_2} \mathrm{d}\varphi' \mathrm{d}\lambda', \end{aligned} \tag{20}$$

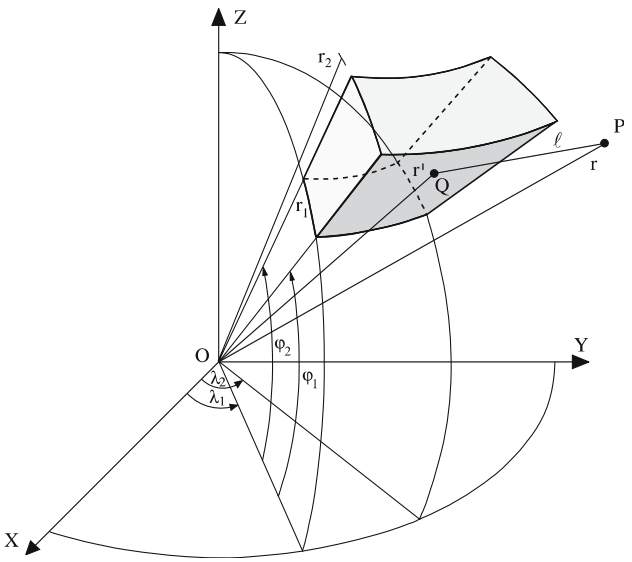

Fig. 4 Geometry of the tesseroid

where the integration over r' is analytically evaluated (cf. Martinec 1998).

Equivalently to MacMillan's (1930) expansion for a prism, a series expansion of Eq. (17) can be used for tesseroids at some distance from the computation point P. Again, maximum efficiency is achieved by fixing the point of the Taylor expansion at the geometrical centre of the tesseroid, i.e. at

$$\begin{aligned} r_o &= (r_1 + r_2)/2, \\ \varphi_o &= (\varphi_1 + \varphi_2)/2, \\ \lambda_o &= (\lambda_1 + \lambda_2)/2. \end{aligned} \tag{21}$$

The Taylor expansion of the integral kernel $r'^2 \cos\varphi'/\ell$ in Eq. (17) can be expressed by

$$\begin{aligned} K(r', \varphi', \lambda') &= \frac{r'^2 \cos\varphi'}{\ell} \\ &= \sum_{i,j,k} K_{ijk} (r' - r_o)^i (\varphi' - \varphi_o)^j (\lambda' - \lambda_o)^k \end{aligned} \tag{22}$$

where

$$K_{ijk} := \frac{1}{(i+j+k)!} \left. \frac{\partial^{i+j+k} K(r', \varphi', \lambda')}{\partial r'^i \partial \varphi'^j \partial \lambda'^k} \right|_{\substack{r'=r_o \\ \varphi'=\varphi_o \\ \lambda'=\lambda_o}} . \tag{23}$$

Inserting Eq. (22) into Eq. (17) yields integrals of the type in Eq. (11), such that only terms with even powers of i, j, and k will remain in the power series (Seitz and Heck 2001; Kuhn and Seitz 2005)

$$\begin{aligned} v(r, \varphi, \lambda) = G\rho \Delta r \Delta\varphi \Delta\lambda \Big[K_{000} + \frac{1}{24} \big(K_{200} \Delta r^2 + K_{020} \Delta\varphi^2 \\ + K_{002} \Delta\lambda^2 \big) + O(\Delta^4) \Big] \end{aligned} \tag{24}$$

where $\Delta r = r_2 - r_1 = h_2 - h_1$, $\Delta\varphi = \varphi_2 - \varphi_1$, $\Delta\lambda = \lambda_2 - \lambda_1$ denote the dimensions of the tesseroid. In Eq. (24), the Landau symbol $O(\Delta^4)$ indicates that terms of order four in $\Delta r, \Delta\varphi, \Delta\lambda$ are omitted. The coefficients K_{ijk} in Eq. (24) depend on the relative positions of the computation point $P(r, \varphi, \lambda)$ and the geometrical centre $P_o(r_o, \varphi_o, \lambda_o)$ of the tesseroid (Taylor point):

$$K_{000} := \frac{r_o^2 \cos\varphi_o}{\ell_o}, \quad \ell_o = \sqrt{r^2 + r_o^2 - 2 r r_o \cos\psi_o} \tag{25}$$

$$\cos\psi_o = \sin\varphi \sin\varphi_o + \cos\varphi \cos\varphi_o \cos(\lambda_o - \lambda). \tag{26}$$

The second-order coefficients K_{200}, K_{020} and K_{002} are given in Appendix A1.

Considering the total mass of the tesseroid

$$\begin{aligned} m &= \rho \int_{\lambda_1}^{\lambda_2} \int_{\varphi_1}^{\varphi_2} \int_{r_1}^{r_2} r'^2 \cos\varphi' \, \mathrm{d}r' \mathrm{d}\varphi' \mathrm{d}\lambda' \\ &= \frac{\rho}{3} \left(r_2^3 - r_1^3 \right) (\sin\varphi_2 - \sin\varphi_1) \Delta\lambda \end{aligned} \tag{27}$$

and the respective series expansion at $P_o(r_o, \varphi_o, \lambda_o)$

$$\begin{aligned} m = \rho r_o^2 \cos\varphi_o \Delta r \Delta\varphi \Delta\lambda \\ \times \left[1 + \frac{1}{12} \left(\frac{\Delta r}{r_o} \right)^2 - \frac{1}{24} (\Delta\varphi)^2 + \cdots \right] \end{aligned} \tag{28}$$

it becomes evident that the zero-order approximation of Eq. (24)

$$\begin{aligned} v(r, \varphi, \lambda) &= \frac{Gm}{\ell_o} \left[1 + O(\Delta^2) \right] \\ &= G\rho \Delta r \Delta\varphi \Delta\lambda K_{000} \left[1 + O(\Delta^2) \right] \end{aligned} \tag{29}$$

is formally identical with the potential of a point mass m placed at P_o, concentrating the total mass of the tesseroid at P_o. The residual terms in Eq. (24) essentially take into account the deviations of the tesseroid from a point-mass.

The effect of the tesseroid mass on the gravity vector at the computation point $P(r, \varphi, \lambda)$ can be calculated by differentiating the integral kernel $1/\ell_o$ in Eqs. (17) or (20) with respect to r, φ and λ. The reduction for the gravitational effect results from

$$\begin{aligned} \delta g &= -\frac{\partial v(r, \varphi, \lambda)}{\partial r} \\ &= G\rho \int_{\lambda_1}^{\lambda_2} \int_{\varphi_1}^{\varphi_2} \int_{r_1}^{r_2} \frac{r'^2 (r - r' \cos\psi) \cos\varphi' \, \mathrm{d}r' \mathrm{d}\varphi' \mathrm{d}\lambda'}{\ell^3} . \end{aligned} \tag{30}$$

Again, integration of Eq. (30) results in elliptic integrals that cannot be solved analytically. Performing the integration with respect to r' the volume integral in Eq. (30) is reduced to the surface integral (cf. Martinec 1998)

$$\begin{aligned} \delta g = \frac{G\rho}{r} \int_{\lambda_1}^{\lambda_2} \int_{\varphi_1}^{\varphi_2} \cos\varphi' \Big[\frac{r'^3}{\ell} - \ell (r' + 3r\cos\psi) - r^2 (3\cos^2\psi - 1) \\ \times \ln(\ell + r' - r\cos\psi) \Big] \Big|_{r'=r_1}^{r'=r_2} \mathrm{d}\varphi' \mathrm{d}\lambda' . \end{aligned} \tag{31}$$

Equations (30) and (31) can be evaluated numerically. As an alternative, the gravitational effect of distant tesseroids can be calculated from a Taylor expansion of

the integral kernel of Eq. (30) at $P_o(r_o, \varphi_o, \lambda_o)$

$$L(r', \varphi', \lambda') = \frac{r'^2\left(r - r'\cos\psi\right)\cos\varphi'}{\ell^3} = \sum_{i,j,k} L_{ijk}\left(r' - r_o\right)^i\left(\varphi' - \varphi_o\right)^j\left(\lambda' - \lambda_o\right)^k \quad (32)$$

where

$$L_{ijk} := \frac{1}{(i+j+k)!}\left.\frac{\partial^{i+j+k}L(r', \varphi', \lambda')}{\partial r'^i \partial\varphi'^j \partial\lambda'^k}\right|_{\substack{r'=r_o \\ \varphi'=\varphi_o \\ \lambda'=\lambda_o}}. \quad (33)$$

Due to our specific choice of the Taylor point P_o, only the terms with even powers of i, j and k remain in the series expansion, which results from inserting Eq. (32) into Eq. (30)

$$\delta g(r, \varphi, \lambda) = G\rho\Delta r\Delta\varphi\Delta\lambda\left[L_{000} + \frac{1}{24}\left(L_{200}\Delta r^2 + L_{020}\Delta\varphi^2 + L_{002}\Delta\lambda^2\right) + O\left(\Delta^4\right)\right]. \quad (34)$$

The coefficients L_{ijk} in Eq. (34) depend on the positions of the computation point $P(r, \varphi, \lambda)$ and the Taylor point $P_o(r_o, \varphi_o, \lambda_o)$. The zero-order coefficient is

$$L_{000} := \frac{r_o^2(r - r_o\cos\psi_o)\cos\varphi_o}{\ell_o^3} = -\frac{\partial K_{000}}{\partial r}. \quad (35)$$

The second-order coefficients $L_{200} = -\frac{\partial K_{200}}{\partial r}, L_{020} = -\frac{\partial K_{020}}{\partial r}$ and $L_{002} = -\frac{\partial K_{002}}{\partial r}$ are presented in Appendix A2.

Again, the zero-order approximation of Eq. (34)

$$\delta g(r, \varphi, \lambda) = \frac{Gm}{\ell_o^3}(r - r_o\cos\psi_o)\left[1 + O\left(\Delta^2\right)\right] = G\rho\Delta r\Delta\varphi\Delta\lambda L_{000}\left[1 + O\left(\Delta^2\right)\right] \quad (36)$$

is essentially identical with the effect of a point-mass m located at P_o on gravitation at P, while the residual terms in Eq. (34) represent the deviations of the tesseroid from a point-mass.

Analogously, the derivatives of the gravitational potential $v(r, \varphi, \lambda)$ with respect to φ and λ will provide the formulas for the (topographic–isostatic) reduction of the vertical deflections at P. It should also be noted that the complete set of formulas derived in this section is valid for computation points situated outside the tesseroid only.

Comparing the sets of formulas for the gravitational effects of a rectangular prism (Sect. 2) and a tesseroid (this section), it becomes clear that – in the case of the tesseroid formulas – no further transformation between different local coordinate systems will be necessary, since the result is already given in the local topocentric system at P; in this respect, the resulting equations are more compact. As such, integration over the complete surface of the Earth or large parts of it can be performed quite efficiently.

The numerical efficiency can even be improved further by calculating the effects of the tesseroids along latitude bands, related to a constant value of φ_o (cf. Smith 2002), where the number of trigonometric function evaluations is reduced greatly. This band-wise approach even allows us to take the Earth's ellipticity into account, just by considering a latitude-dependent Earth radius in r_o: Instead of the mean radius R the prime vertical radius N_o

$$N_o := \frac{a}{\sqrt{1 - e^2\sin^2\varphi_o}} \quad (37)$$

(a: semi-major axis, e: first numerical eccentricity of the Earth ellipsoid) in the latitude band φ_o = const can be used. In the ellipsoidal case, φ and φ_o are geodetic latitudes.

4 Numerical investigations

To get an impression of the advantage using tesseroids instead of prisms or point-masses, several numerical tests have been performed. The comparisons refer to the required computation time, the achievable precision and the approximation error, considering gravitational potential and attraction.

According to Eq. (28), the dimensions of the "equivalent" rectangular prism are computed from the dimensions of the tesseroid. This implies mass equivalence of the first-order under the further assumption that the tesseroid and the prism have the same constant mass-density ρ:

$$m_{\text{tesseroid}} = m_{\text{prism}}$$
$$\rho r_o^2\cos\varphi_o\Delta r\Delta\varphi\Delta\lambda\left[1 + \frac{1}{12}\left(\frac{\Delta r}{r_o}\right)^2 - \frac{1}{24}(\Delta\varphi)^2 + \cdots\right] = \rho\Delta x\Delta y\Delta z. \quad (38)$$

Neglecting terms of order $O\left(\Delta^2\right)$and identifying the spherical height of the tesseroid with the height of the prism

$$\Delta z = \Delta r \quad (39a)$$

the horizontal dimensions of the prism are fixed as

$$\Delta x = r_o\Delta\varphi \quad (39b)$$
$$\Delta y = r_o\cos\varphi_o\Delta\lambda. \quad (39c)$$

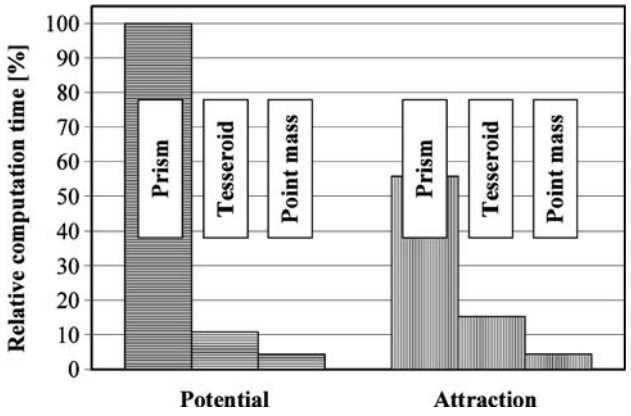

Fig. 5 Comparison of the computation time using tesseroid, prism or point mass to compute potential and gravitational attraction

The approximation error induced by neglecting terms of order $O(\Delta^2)$ in Eq. (38) depends on the size of the tesseroid; the maximum relative error in the volume, gravitational potential and gravitational acceleration of a tesseroid can be estimated as 10^{-5} for $|\Delta\varphi| = 1°$ and 10^{-7} for $|\Delta\varphi| = 5'$ and $|\Delta\, \mathrm{r}| \leq 9{,}000\,\mathrm{m}$.

To compare the respective computation time the JGP95E global DTM (Lemoine et al. 1998, Chap. 2) was used as a realistic test field. It is related to a $5' \times 5'$ global grid in geodetic coordinates (here assumed spherical) and consists of $2{,}160 \times 4{,}320 = 9{,}331{,}200$ tesseroids. At each centre point on the upper surface of a grid element, the effect of all tesseroids on potential and gravity has been computed. It is obvious from Fig. 4 that the topography ($r_1 = R, r_2 = R + H$) or the residual topography ($r_1 = R + H_1, r_2 = R + H_2$) can be modelled with the aid of tesseroids, for example, in the framework of terrain reduction. The following test computations have been carried out for terrain reductions; here, the difference between ellipsoidal and orthometric heights (i.e. the geoid height) has been neglected.

For each computation point P, the tesseroids are bounded in the vertical direction by concentric spheres of radii $r_1 = R + H_P$ and $r_2 = R + H_{ij}$, where H_{ij} denotes the topographic height of the DTM grid element (i, j). As a consequence, there is no contribution from the central element ($H_P = H_{ij}; \Delta r = 0$) to the terrain reduction. The comparison among the required computation times for the evaluation of the gravitational potential and gravitational acceleration from a tesseroid, prism and point-mass from the JGP95E DTM is visualized in Fig. 5

Concerning the computation time required to evaluate the potential values, one can notice from Fig. 5 that the algorithm applied for the computation of the potential of the tesseroids runs 10 times faster than that implemented for the prisms. This remarkable difference is caused by time-consuming 24 *log* and 24 *arctan* function calls per prism. With respect to the point-mass approximation, the tesseroids are slower only by a factor of two. In extensive numerical evaluations, the point-mass approximation may be used to compute the far zone contributions, but in general the tesseroids should be preferred.

The gain of efficiency is reduced when the necessary computation time regarding the gravitational attraction is compared (Fig. 5). The computation of the attraction by a prism takes only half of the time in comparison with the gravitational potential of a prism. This is caused by the fact that the number of function calls decreases; to compute the attraction of a prism in the local coordinate system of the computation point 12 *log* and 24 *arctan* function calls per prism are required. In comparison to the tesseroids, there is still a factor of four.

The absolute accuracy of the respective discretisation approach (prism, tesseroid, point-mass) and the associated approximation error for gravitational potential and attraction can only be analysed in comparison with a mass distribution where an analytical solution exists. This is the case for a spherical cap of constant thickness $d = r_2 - r_1$, constant mass-density ρ and constant radius ψ_c, centred at the computation point. The spherical angle ψ counts from the geocentric direction of the computation point $P(r, \psi = 0°)$, which actually coincides with the origin of the spherical coordinate system.

The formulas for the gravitational potential of a cap at the computation point $p(r, \psi = 0°)$ are

$$\begin{aligned} &v(r; r_1, r_2, \psi_c) \\ &\quad = 2\pi G\rho \left\{ \frac{1}{3r}\ell_c'^3 + \frac{1}{2}\ell_c' \cos\psi_c \left(r' - r\cos\psi_c\right) \right. \\ &\qquad \left. + \frac{1}{2} r^2 \cos\psi_c \sin^2\psi_c \ln\left(\ell_c' + r' - r\cos\psi_c\right) \right\} \Bigg|_{r'=r_1}^{r'=r_2} \\ &\qquad + 2\pi G\rho \left(+\frac{1}{3r} r'^3 - \frac{1}{2} r'^2 \right) \Bigg|_{r'=r_1}^{r'=r_2} \begin{cases} +1 & r \geqslant r_2 \\ -1 & r \leqslant r_1 \end{cases}, \end{aligned} \tag{40}$$

where $\ell_c' = \sqrt{r^2 + r'^2 - 2rr'\cos\psi_c}$, and for the gravitational attraction of a cap, they are

$$\begin{aligned} &\delta g(r; r_1, r_2, \psi_c) \\ &\quad = -\frac{\partial v(r; r_1, r_2, \psi_c)}{\partial r} \\ &\quad = 2\pi G\rho \left\{ -\frac{1}{3r^2}\ell_c'^3 + \frac{1}{r}\ell_c'\left(r - r'\cos\psi_c\right) - \frac{1}{2}\ell_c' \cos^2\psi_c \right. \\ &\qquad + \frac{1}{2}\cos\psi_c \left(r' - r\cos\psi_c\right) \frac{r - r'\cos\psi_c}{\ell_c'} \\ &\qquad \left. + r\cos\psi_c \sin^2\psi_c \ln\left(\ell_c' + r' - r\cos\psi_c\right) \right. \end{aligned}$$

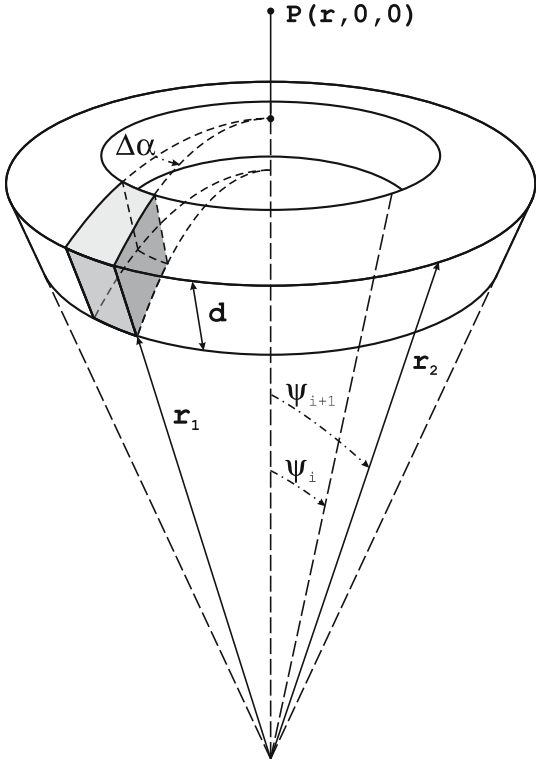

Fig. 6 Geometry of a spherical zonal band and a tesseroid

$$+\frac{1}{2}r^2\cos\psi_c\sin^2\psi_c\frac{r-(\ell'_c+r')\cos\psi_c}{\ell'_c(\ell'_c+r'-r\cos\psi_c)}\Bigg\}\Bigg|_{r'=r_1}^{r'=r_2}$$
$$+2\pi G\rho\left(-\frac{1}{3r^2}r'^3\right)\Bigg|_{r'=r_1}^{r'=r_2}\begin{cases}+1, & r\geqslant r_2\\ -1, & r\leqslant r_1\end{cases}, \tag{41}$$

see the derivation in Appendices A3 and A4.

From the analytical solutions of the gravitational potential (Eq. 40) and gravitational attraction (Eq. 41) of a spherical cap, where the computation point is located at the origin of the spherical polar coordinate system, the potential and attraction of a spherical zonal band between the spherical distances ψ_i and ψ_{i+1} (Fig. 6) can be derived from

$$v(r;r_1,r_2,\psi_i,\psi_{i+1})=v(r;r_1,r_2,\psi_{i+1})-v(r;r_1,r_2,\psi_i) \tag{42a}$$
$$\delta g(r;r_1,r_2,\psi_i,\psi_{i+1})=\delta g(r;r_1,r_2,\psi_{i+1})-\delta g(r;r_1,r_2,\psi_i). \tag{42b}$$

In the following, the analytical solutions for the potential and attraction of spherical ring zones of constant height and band-width $\Delta\psi$ are used as absolute values for comparison.

The numerical solutions resulting from the point-mass, prism and tesseroid approximations for these zonal bands are compared in Figs. 7a, b with the analytical values from Eq. (42a), respectively. The tesseroid dimensions in each spherical zonal band of band-width $\Delta\psi = \psi_{i+1} - \psi_i = 5'$ with $0 \leqslant \psi_i < \psi_{i+1} \leqslant \pi$ have been chosen as $\Delta\alpha = 5'$ (azimuthal difference) and $d = H = r_2 - r_1 = 1,000\,\mathrm{m}$ (height). Due to the rapid decrease of the approximation errors with spherical distance ψ_i, the results are plotted in logarithmic scale. Besides the absolute values of the approximation errors, the analytical values of the contribution of each concentric spherical zonal band is plotted (dashed line in Fig. 7) to show the relative accuracy.

Remark The prism formulas (Eqs. 4 and 6) are exact analytical solutions for a homogeneous prism. However, under the assumption of mass equality, the dimensions of the prisms have to be calculated from the extension of the tesseroids, since in practice a DTM is mostly given in geodetic coordinates (here assumed spherical). Therefore, the prism method also produces an approximation error in the present test example of spherical ring zones, caused by the different geometry of a prism and a tesseroid on the one hand and – to a minor extent – the approximated mass balance (Eq. (39b)) on the other hand. In particular, for small distances ψ_i, the shapes of a tesseroid and a prism of equal volume are very different; in the direct vicinity of the computation point, the tesseroid degenerates and has a triangular base shape. For details, see Grüninger (1990) and Kuhn (2000).

The analytical solution of the gravitational potential and attraction of a concentric spherical zonal band composed of the difference between two successive spherical caps shows a nearly constant behaviour in the plotted region $0 \leqslant \psi_i \leqslant 10°$, the near-zone of the computation point. This can be explained by the fact that the mass within a spherical zonal band (here, $\Delta\psi = 5' = \mathrm{const}$) is increasing in a nearly linear manner with increasing distance ψ_i to the computation point. However, the reciprocal decrease of the potential with increasing distance counteracts this behaviour; the result is an approximately constant contribution of each concentric zonal band up to a spherical distance of about $\psi_i = 10°$ (see Fig. 7, upper curve).

The reasoning for the behaviour of the gravitational attraction is analogous: the decrease with the square of the distance is counteracted by the linearly increasing volume in the calculation of the vertical component of the gravitational attraction at the computation point (Fig. 7b, upper curve). It can be recognized from Fig. 7a, b that the decay of the approximation error with increasing distance of the spherical ring zone is much faster for the tesseroid in comparison with the prism and point-

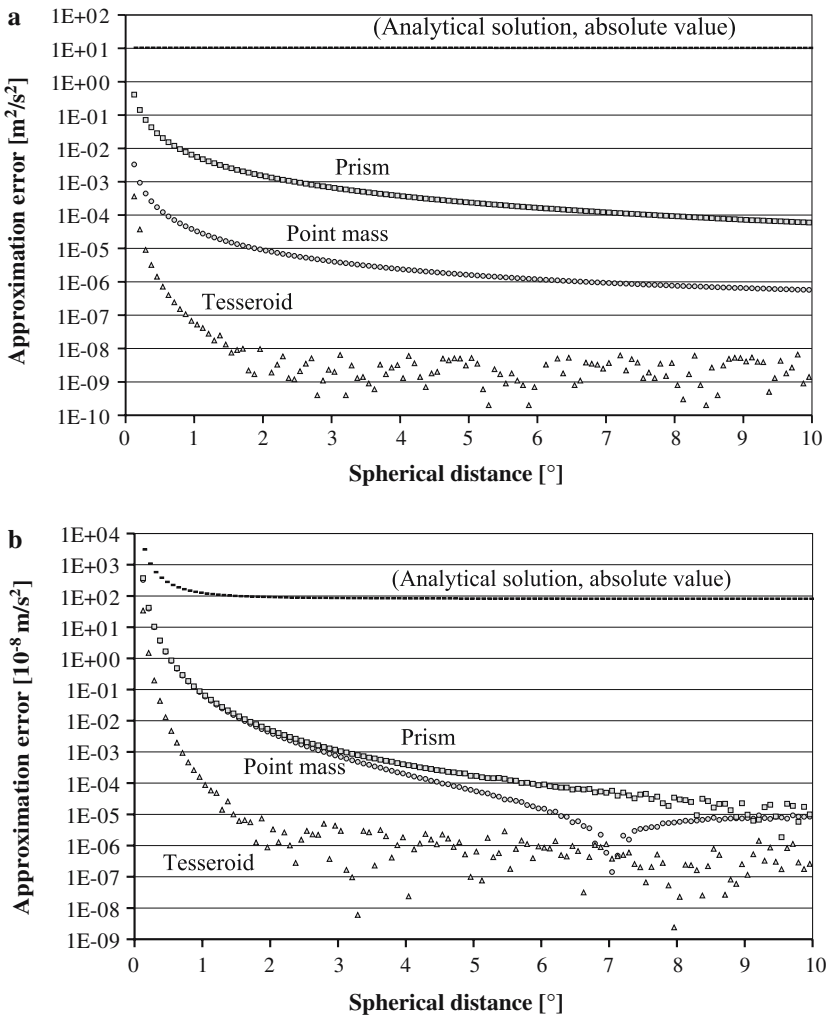

Fig. 7 **a** Analytical solution and approximation error of the potential of a zonal band ($\Delta\psi = 5'$) using tesseroid, prism or point-mass ($\Delta\alpha = 5',\ H = 1{,}000\,\text{m}$). **b** Analytical solution and approximation error of the gravitational attraction of a zonal band ($\Delta\psi = 5'$) using tesseroid, prism or point-mass ($\Delta\alpha = 5',\ H = 1{,}000\,\text{m}$)

mass approximations. When the spherical distance is greater than about 1.5°, the error is mainly induced by rounding errors of the computer (single precision IEEE arithmetic). In contrast, the prism and point-mass approximations still produce significant errors for $\psi_i = 10°$ (potential) and 5° (attraction). The behaviour of the point-mass approximation at $\psi_i \approx 7°$ can be explained by a change of sign of the error from positive to negative values.

In a further test, the computation point is located at the equator $P(r, \varphi = 0°, \lambda = 0°)$, the integration area is defined as $-1° = \varphi_{\min} \leqslant \varphi_{ij} \leqslant \varphi_{\max} = +1°$ and $-1° = \lambda_{\min} \leqslant \lambda_{ij} \leqslant \lambda_{\max} = +1°$. The height of the mass element is equal to the height of the computation point, $h_P = h_{ij} = 100\,\text{m}$. In this test example, an exact analytical solution for the calculation of the gravitational potential and gravitation of the $2° \times 2°$ mass configuration is not available. As such, only the numerical results for the tesseroid, prism and point-mass approximations can be compared.

In order to check the approximation error due to the truncation of the Taylor series expansion (Eqs. 24 and 34), the integration area was gridded with tesseroids of various grid sizes. The results obtained, depending on the regular grid spacing $\Delta\varphi = \Delta\lambda$, are shown in Fig. 8 From Fig. 8a, it can be stated that a spacing less than $\Delta\varphi = \Delta\lambda = 60$" causes errors in the potential less than $0.1\,\text{m}^2/\text{s}^2$ for the total $2° \times 2°$ block. A coarse spacing of 0.5° or 1° causes unacceptable errors for the point-mass and tesseroid modelling.

The behaviour of the gravitational attraction is shown in Fig. 8b. The computed attraction for the prisms converge very fast to a fixed value for a spacing less than 60". The results for point masses and tesseroids converge very slowly when the grid size decreases.

As can be concluded from Fig. 9, where the four elements located in the immediate vicinity of the computation point are eliminated, the approximation error due to the truncation of the Taylor expansion decreases very quickly depending on the distance to the computation

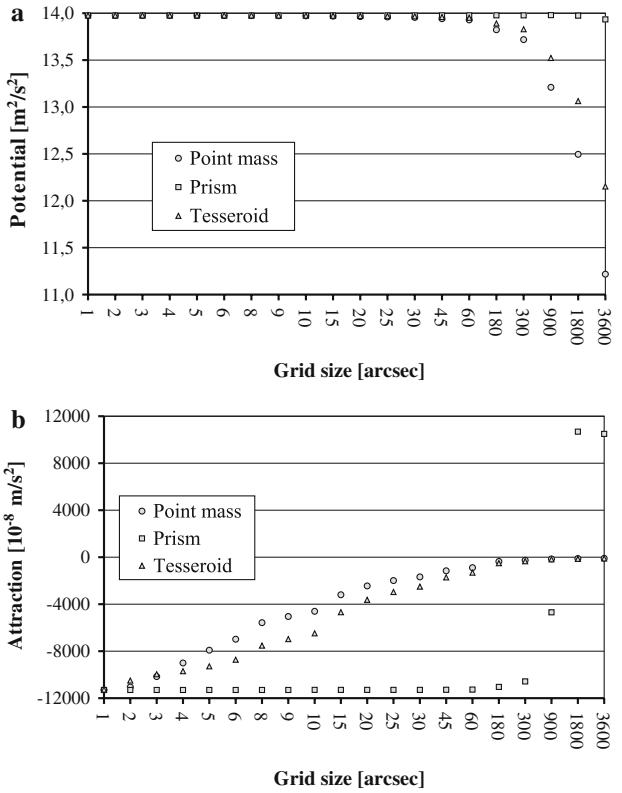

Fig. 8 **a** Computation of the gravitational potential at P_{Equator} induced by the area $-1^\circ = \varphi_{\min} \leqslant \varphi_{ij} \leqslant \varphi_{\max} = +1^\circ$ and $-1^\circ = \lambda_{\min} \leqslant \lambda_{ij} \leqslant \lambda_{\max} = +1^\circ (H = 100\,\mathrm{m})$ depending on the grid size $\Delta\varphi = \Delta\lambda$. **b** Computation of the gravitational attraction at P_{Equator} induced by the area $-1^\circ = \varphi_{\min} \leqslant \varphi_{ij} \leqslant \varphi_{\max} = +1^\circ$ and $-1^\circ = \lambda_{\min} \leqslant \lambda_{ij} \leqslant \lambda_{\max} = +1^\circ (H = 100\,\mathrm{m})$ depending on the grid size $\Delta\varphi = \Delta\lambda$

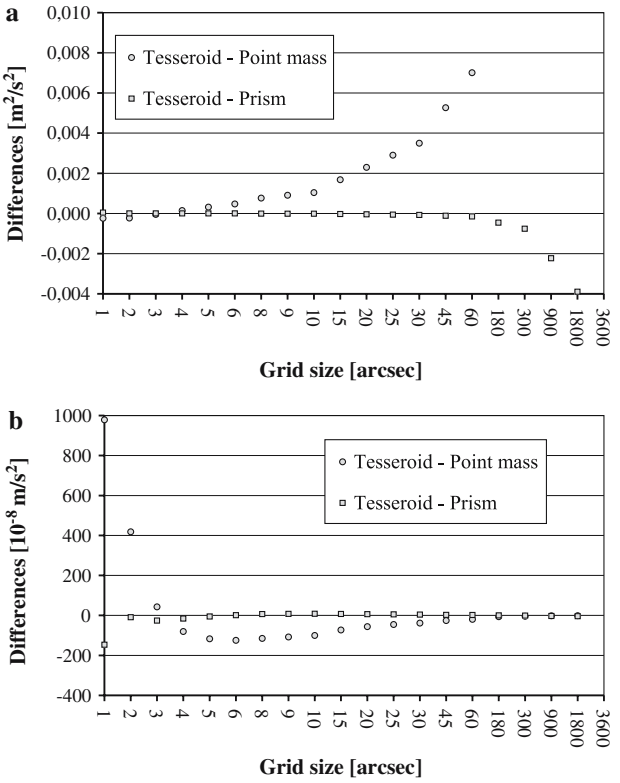

Fig. 9 **a** Computation of the gravitational potential at P_{Equator} induced by the area $-1^\circ = \varphi_{\min} \leqslant \varphi_{ij} \leqslant \varphi_{\max} = +1^\circ$ and $-1^\circ = \lambda_{\min} \leqslant \lambda_{ij} \leqslant \lambda_{\max} = +1^\circ (H = 100\,\mathrm{m})$ omitting the four elements nearest to the computation point. **b** Computation of the gravitational attraction at P_{Equator} induced by the area $-1^\circ = \varphi_{\min} \leqslant \varphi_{ij} \leqslant \varphi_{\max} = +1^\circ$ and $-1^\circ = \lambda_{\min} \leqslant \lambda_{ij} \leqslant \lambda_{\max} = +1^\circ (H = 100\,\mathrm{m})$ omitting the four elements nearest to the computation point

point. It is evident that the slow convergence demonstrated in Fig. 8 is caused by the error induced by the elements located in the direct vicinity of the computation point.

The reason for this behaviour can be found in the redistribution of the mass when the tesseroid is replaced by an "equivalent" point mass or prism. This effect is larger when the distance of the mass element to the computation point decreases, and is much more pronounced for point masses. Furthermore, the approximation errors for the prismatic bodies are partly induced by replacing the curved upper and lower surfaces of the tesseroid by planes. A part of the difference for small grid size, visualized in Fig. 9, is due to the truncation error in the tesseroid formulas (Eqs. 24 and 34), resulting from the Taylor expansion. In this test example, the results for the tesseroid and prism approximations are quite similar, which can be explained by the fact that the geometrical shape of these bodies is nearly the same.

5 Conclusions

By partitioning the topographic (or isostatic) masses into tesseroids, i.e. geometrical bodies bounded by geographic grid lines and surfaces of constant height, an efficient procedure has been proposed for mass reductions in gravity field modelling. Since the volume integrals for the calculation of the gravitational potential and attraction effects cannot be evaluated analytically, a Taylor series expansion of the integral kernels is used. By choosing the geometrical centre of the tesseroid as the Taylor point, the number of non-vanishing series terms is greatly reduced.

A comparison of the tesseroid formulas with the traditional prism method shows that the calculation speed is improved by a factor of 10 for the gravitational potential and a factor of 4 for gravitational acceleration. For global numerical evaluations, the efficiency can be increased further by working in latitude bands and considering recurrence formulas for the calculation of

trigonometric functions. The sphericity of the Earth is automatically taken into account in the tesseroid approach, while the curvature effect and the inclination of the mass elements have to be considered separately in the prism approach in an approximate manner.

Reducing the series expansion to the zero-order term results in the point-mass formula; the additional second-order terms represent the relative dimensions of the tesseroid. In some respects, the proposed procedure resembles MacMillan's (1930) approach, which is based on similar series expansions for prismatic bodies, where the zero-order term is also equivalent to the point mass formula.

The precision of the tesseroid procedure has been checked with the aid of a test scenario based on the gravitational potential and attraction of a spherical cap of constant mass-density and thickness. If the computation point is situated on the symmetry axis of the spherical cap, the volume integrals for the potential and gravity can be analytically (i.e. exactly) solved. The dependence of the precision on the distance of the mass elements has been evaluated by considering the effect of concentric zonal bands, arising from the difference between the caps of subsequent radii.

From this, while the approximation error for the second-order tesseroid formula decreases very quickly with increasing distance to the computation point, the decay is much slower for the prism method and for the point-mass formula. Close to the computation point, the results are sensitive to the shape of the model body used. In the direct vicinity of the computation point, the "rectangular" tesseroid degenerates and possesses a triangular base shape; the approximation of those bodies by rectangular prisms or point-masses produces large errors. For increasing distance from the computation point, the point-mass and prism approximations become better and better. It should be noted that the prism routine breaks down for large distances, due to the loss of significant digits when the required functions are evaluated for nearly the same arguments, and differences are taken as required.

In a second experiment, the computation point was placed at the equator, at the centre of a $2^\circ \times 2^\circ$ massive block. Here, the tesseroids in the neighbourhood of the computation point have a nearly quadratic base, and the approximation by prisms produces rather good results, in particular for DTM side lengths less than 60". From this numerical experiment, it becomes clearly visible that the use of the second-order tesseroid formula produces unacceptable errors, in particular for the calculation of the effect on gravitational attraction; the errors induced by the point-mass formula are even larger. As a conclusion, the effect of the mass elements in the vicinity of the computation point should be calculated using the prism formulas.

The results presented here for spherical tesseroids can easily be transferred to the ellipsoidal case: the Earth's ellipticity can be taken into account by considering a latitude-dependent Earth radius, e.g. the prime vertical radius of the ellipsoid. This procedure can be combined with the calculation on latitude bands, as mentioned earlier.

Acknowledgements The authors wish to thank Dr Dezsö Nagy, Dr Gabor Papp and another anonymous reviewer, as well as the Editor-in-Chief, for valuable remarks, which helped to clarify some topics and to improve the presentation.

Appendix A

A1 Second-order coefficients K_{200}, K_{020} and K_{002} according to Eq. (24)

$$K_{200} = \frac{r^2 \cos\varphi_o}{\ell_o^5}\left\{2\ell_o^2 - 3r_o^2 \sin^2\psi_o\right\} \tag{43}$$

$$\begin{aligned} K_{020} = \frac{r_o^2}{\ell_o^5}\Big\{&-\cos\varphi_o\left(r^2+r_o^2\right)\left[r^2 + r_o^2 - rr_o\sin\varphi\sin\varphi_o\right] \\ &+r^2 r_o^2\cos\varphi_o\Big[\sin^2\varphi\left(3-\sin^2\varphi_o\right) - \cos^2\varphi \\ &\times\left(2-\sin^2\varphi_o\right)\cos^2\delta\lambda\Big] + rr_o\cos\varphi\left(3-\sin^2\varphi_o\right) \\ &\times\left[r^2 + r_o^2 - 2rr_o\sin\varphi\sin\varphi_o\right]\cos\delta\lambda\Big\} \end{aligned} \tag{44}$$

$$\begin{aligned} K_{002} = &-\frac{rr_o^3\cos\varphi\cos^2\varphi_o}{\ell_o^5} \\ &\times\left\{\ell_o^2\cos\delta\lambda - 3rr_o\cos\varphi\cos\varphi_o\sin^2\delta\lambda\right\} \end{aligned} \tag{45}$$

with $\delta\lambda = \lambda_o - \lambda$.

A2 Second-order coefficients L_{200}, L_{020} and L_{002} according to Eq. (34)

$$\begin{aligned} L_{200} &= -\frac{\partial K_{200}}{\partial r} \\ &= \frac{r\cos\varphi_o}{\ell_o^3}\left\{2 - \frac{3r_o}{\ell_o^2}\left[5r_o - (2r + 3r_o\cos\psi_o)\cos\psi_o\right]\right. \\ &\qquad \left. + \frac{15r_o^3}{\ell_o^4}\sin^2\psi_o(r_o - r\cos\psi_o)\right\} \end{aligned} \tag{46}$$

$$L_{020} = -\frac{\partial K_{020}}{\partial r}$$

$$
\begin{aligned}
&= \left(\frac{r_o}{\ell_o}\right)^3 \cos\varphi\left(1-2\sin^2\varphi_o\right)\cos\delta\lambda \\
&\quad + \frac{r_o^2}{\ell_o^5}\Big\{-r\left(r^2+r_o^2\right)\cos\varphi_o \\
&\qquad + r_o\sin\varphi\Big[-rr_o\left(\sin\varphi\cos\varphi_o-\cos\varphi\sin\varphi_o\cos\delta\lambda\right) \\
&\qquad + \sin\varphi_o\cos\varphi_o\left(2r^2+4r_o^2-3rr_o\sin\varphi\sin\varphi_o\right)\Big] \\
&\qquad + r_o^2\cos\varphi\cos\delta\lambda\left(1-2\sin^2\varphi_o\right) \\
&\qquad \times\left[r_o+r\cos\varphi\cos\varphi_o\cos\delta\lambda\right] \\
&\qquad + rr_o^2\cos\varphi\sin\varphi_o\cos\varphi_o\cos\delta\lambda \\
&\qquad \left[3\sin\varphi\cos\varphi_o-4\cos\varphi\sin\varphi_o\cos\delta\lambda\right]\Big\} \\
&\quad + \frac{5rr_o^3}{\ell_o^7}\Big\{-r\left(r^2+r_o^2\right)\sin\varphi_o \\
&\qquad\quad + r_o^2\cos\varphi\sin\varphi_o\cos\varphi_o\cos\delta\lambda \\
&\qquad\quad \times\left(r_o+r\cos\varphi\cos\varphi_o\cos\delta\lambda\right) \\
&\qquad\quad + r_o\sin\varphi\Big[2r^2-r_o^2-rr_o\cos\psi_o+\sin^2\varphi_o \\
&\qquad\quad \times\left(r^2+2r_o^2-rr_o\sin\varphi\sin\varphi_o\right)\Big]\Big\} \\
&\quad \times\left(\sin\varphi\cos\varphi_o-\cos\varphi\sin\varphi_o\cos\delta\lambda\right) \qquad (47)
\end{aligned}
$$

$$
\begin{aligned}
L_{002} &= -\frac{\partial K_{002}}{\partial r} \\
&= \left(\frac{r_o}{\ell_o}\right)^3 \cos\varphi\cos^2\varphi_o \\
&\quad \times\Big\{\cos\delta\lambda-\frac{3r}{\ell_o^2}\Big[2r_o\cos\varphi\cos\varphi_o\sin^2\delta\lambda \\
&\qquad + (r-r_o\cos\psi_o)\cos\delta\lambda\Big] \\
&\qquad + \frac{15r^2r_o}{\ell_o^4}\cos\varphi\cos\varphi_o\left(r-r_o\cos\psi_o\right)\sin^2\delta\lambda\Big\}
\end{aligned} \qquad (48)
$$

A3 The gravitational potential $v(r;r_1,r_2,\psi_c)$ of a spherical cap

The gravitational potential v of a spherical cap of homogeneous mass-density ρ is described by Newton's integral

$$
v(r;r_1,r_2,\psi_c) = G\rho\int_0^{2\pi}\int_0^{\psi_c}\int_{r_1}^{r_2}\frac{r'^2\sin\psi'\,\mathrm{d}r'\,\mathrm{d}\psi'\,\mathrm{d}\alpha'}{\ell} \qquad (49)
$$

where the Euclidean distance ℓ between the computation point $P(r,\psi=0°)$ and the running integration point $Q(r',\psi',\alpha')$ is defined in Eq. (18). Integration with respect to the azimuth α' for the rotationally symmetrical cap results in

$$
v(r;r_1,r_2,\psi_c) = 2\pi G\rho\int_0^{\psi_c}\int_{r_1}^{r_2}\frac{r'^2\sin\psi'\,\mathrm{d}r'\,\mathrm{d}\psi'}{\sqrt{r^2+r'^2-2rr'\cos\psi'}} \qquad (50)
$$

and integration with respect to the spherical distance ψ' yields

$$
\begin{aligned}
v(r;r_1,r_2,\psi_c) = \frac{2\pi G\rho}{r}\int_{r_1}^{r_2}\Big\{&\sqrt{r^2+r'^2-2rr'\cos\psi_c} \\
&-\left|r-r'\right|\Big\}\,r'\,\mathrm{d}r'.
\end{aligned} \qquad (51)
$$

Finally, after the radial integration, the formula for the gravitational potential of a spherical cap is given by (cf. Papp and Wang 1996; Martinec 1998)

$$
\begin{aligned}
&v(r;r_1,r_2,\psi_c) \\
&= 2\pi G\rho\Big\{\frac{1}{3r}\ell_c'^3+\frac{1}{2}\ell_c'\cos\psi_c\left(r'-r\cos\psi_c\right) \\
&\qquad + \frac{1}{2}r^2\cos\psi_c\sin^2\psi_c\ln\left(\ell_c'+r'-r\cos\psi_c\right)\Big\}\Big|_{r'=r_1}^{r'=r_2} \\
&\qquad + 2\pi G\rho\left(+\frac{1}{3r}r'^3-\frac{1}{2}r'^2\right)\Big|_{r'=r_1}^{r'=r_2}\begin{cases}+1 & r\geqslant r_2\\ -1 & r\leqslant r_1\end{cases},
\end{aligned} \qquad (52)
$$

where $\ell_c' = \sqrt{r^2+r'^2-2rr'\cos\psi_c}$.

If the extension of the cap tends in the limit to $\psi_c=\pi$, the gravitational potential of a spherical shell of constant mass-density ρ follows from Eq. (52) (cf. Vaníček et al. 2001, 2004):

$$
v(r;r_1,r_2) = \begin{cases}\frac{4\pi G\rho}{3r}\left(r_2^3-r_1^3\right), & r\geqslant r_2\\ 2\pi G\rho\left(r_2^2-r_1^2\right), & r\leqslant r_1\end{cases}. \qquad (53)
$$

A4 The gravitational attraction $\delta g(r;r_1,r_2,\psi_c)$of a spherical cap

The gravitational attraction at the computation point $P(r,\psi=0°)$ caused by the spherical cap can be derived from Eq. (52) by differentiation with respect to the radial

direction r:

$$\begin{aligned}
&\delta g(r;r_1,r_2,\psi_c)\\
&\quad=-\frac{\partial v(r;r_1,r_2,\psi_c)}{\partial r}\\
&\quad=2\pi G\rho\left\{-\frac{1}{3r^2}\ell_c'^3+\frac{1}{r}\ell_c'\left(r-r'\cos\psi_c\right)-\frac{1}{2}\ell_c'\cos^2\psi_c\right.\\
&\qquad+\frac{1}{2}\cos\psi_c\left(r'-r\cos\psi_c\right)\frac{r-r'\cos\psi_c}{\ell_c'}\\
&\qquad+r\cos\psi_c\sin^2\psi_c\ln\left(\ell_c'+r'-r\cos\psi_c\right)\\
&\qquad\left.+\frac{1}{2}r^2\cos\psi_c\sin^2\psi_c\frac{r-\left(\ell_c'+r'\right)\cos\psi_c}{\ell_c'\left(\ell_c'+r'-r\cos\psi_c\right)}\right\}\Bigg|_{r'=r_1}^{r'=r_2}\\
&\quad+2\pi G\rho\left(-\frac{1}{3r^2}r'^3\right)\Bigg|_{r'=r_1}^{r'=r_2}\begin{cases}+1, & r\geqslant r_2\\ -1, & r\leqslant r_1\ .\end{cases}
\end{aligned}\tag{54}$$

The gravitational attraction of a spherical shell results from Eq. (54) with $\psi_c=\pi$ (cf. Vaníček et al. 2001, 2004):

$$\delta g(r;r_1,r_2)=-\frac{4\pi G\rho}{3r^2}\begin{cases}r_2^3-r_1^3, & r\geqslant r_2\\ 0, & r\leqslant r_1\ .\end{cases}\tag{55}$$

If terms of the order d/r and H/r with $d=r_2-r_1$ and $H=r-r_1$ are neglected, the gravitational attraction of a spherical shell with constant mass-density ρ is approximated by

$$\delta g(r;r_1,r_2)\doteq-4\pi G\rho d,\quad r\geqslant r_2>r_1\,.\tag{56}$$

This is twice the effect of an infinite planar Bouguer plate (Vaníček et al. 2001).

References

Anderson EG (1976) The effect of topography on solutions of Stokes' problem. Unisurv S-14, Rep, School of Surveying, University of New South Wales, Kensington

Forsberg R (1984) A study of terrain reductions, density anomalies and geophysical inversion methods in gravity field modelling. Rep 355, Department of Geodetic Science, The Ohio State University, Columbus

Forsberg R (1985) Gravity field terrain effect computations by FFT. Bull Géod 59:342–360

Forsberg R, Sideris MG (1989) On topographic effects in gravity field approximation. In: Kejlsø E, Poder K, Tscherning CC (eds) Festschrift to Torben Krarup. Geodaetisk Institut Meddelelse No 58, København, pp 129–148

Forsberg R, Tscherning CC (1997) Topographic effects in gravity field modelling for BVP. In: Sansò F, Rummel R (eds) Geodetic boundary value problems in view of the one centimetre geoid. Lecture Notes in Earth Sciences, vol 65. Springer, Berlin Heidelberg New York, pp 241–272

Grüninger W (1990) Zur topographisch-isostatischen Reduktion der Schwere. PhD Thesis, Universität Karlsruhe

Hackney RI, Featherstone WE (2003) Geodetic versus geophysical perspective of the 'gravity anomaly'. Geophys J Int 154(1):35–43, erratum in 154(2):596

Hammer S (1939) Terrain corrections for gravimeter stations. Geophysics 4:184–194

Harrison JC, Dickinson M (1989) Fourier transform methods in local gravity field modelling. Bull Géod 63:149–166

Heck B (2003a) On Helmert's methods of condensation. J Geod 77(3–4):155–170, DOI: 10.1007/s00190-003-0318-5

Heck B (2003b) Rechenverfahren und Auswertemodelle der Landesvermessung. Klassische und moderne Methoden, 3rd edn. Wichmann, Heidelberg

Heiskanen WA, Moritz H (1967) Physical geodesy. Freeman, San Francisco

Heiskanen WA, Vening Meinesz FA (1958) The Earth and its gravity field. McGraw-Hill, New York

Jekeli C, Serpas JG (2003) Review and numerical assessment of the direct topographical reduction in geoid determination. J Geod 77(3–4):226–239, DOI: 10.1007/s00190-003-0320-y

Jung K (1961) Schwerkraftverfahren in der Angewandten Geophysik. Akademische Verlagsgesellschaft. Geest& Portig, Leipzig

Klose U, Ilk KH (1993) A solution to the singularity problem occurring in the terrain correction formula. Manuscr Geod 18:263–279

Koch KR (1965) Die topographische Schwere- und Lotabweichungsreduktion für Aufpunkte in geneigtem Gelände. Allg Vermess.-Nachr 11:438–441

Kuhn M (2000) Geoidbestimmung unter Verwendung verschiedener Dichtehypothesen. Reihe C, Heft Nr 520. Deutsche Geodätische Kommission, München

Kuhn M, Seitz K (2005) Comparison of Newton's integral in the space and frequency domains. In: Sansò F (ed) A window on the future of geodesy. Proceedings of the IAG General Assembly, Sapporo, Japan 2003. IAG Symposia, vol 128. Springer, Berlin Heidelberg New York, pp 386–391

LaFehr TR (1991a) Standardization in gravity reduction. Geophysics 56(8):1170–1178

LaFehr TR (1991b) An exact solution for the gravity curvature (Bullard B) corrections. Geophysics 56 (8):1179–1184

Lemoine FG, Kenyon SC, Factor JK, Trimmer RG, Pavlis NK, Chinn DS, Cox CM, Klosko SM, Luthcke SB, Torrence MH, Wang YM, Williamson RG, Pavlis EC, Rapp RH and Olson TR (1998) The development of the joint NASA GSFC and the National Imagery and Mapping Agency (NIMA) geopotential model EGM96. Report TP-1998–206861, NASA Goddard Space Flight Center, Greenbelt, 575 pp

Li YC, Sideris MG (1994) Improved gravimetric terrain corrections. Geophys J Int 119:740–752

MacMillan WD (1930) Theoretical Mechanics, vol 2: the Theory of the potential. McGraw-Hill, New York (reprinted by Dover Publications, New York 1958)

Mader K (1951) Das Newtonsche Raumpotential prismatischer Körper und seine Ableitungen bis zur dritten Ordnung. Österr Z Vermess Sonderheft, vol 11

Martinec Z (1998) Boundary value problems for gravimetric determination of a precise geoid. Lecture notes in Earth Sciences, vol 73. Springer, Berlin Heidelberg New York

Martinec Z, Vaníček P, Mainville A and Véronneau M (1996) Evaluation of topographical effects in precise geoid computation from densely sampled heights. J Geod 70(11):746–754, DOI: 10.1007/BF00867153

Moritz H (1968) On the use of the terrain correction in solving Molodensky's problem. Rep 108, Department of Geodetic Science, The Ohio State University, Columbus

Moritz H (1980) Advanced physical geodesy. Wichmann, Karlsruhe

Nagy D (1966) The gravitational attraction of a right rectangular prism. Geophysics 31:362–371

Nagy D, Papp G, Benedek J (2000) The gravitational potential and its derivatives for the prism. J Geod 74(7–8):552–560, DOI: 10.1007/s001900000116

Nagy D, Papp G, Benedek J (2002) Corrections to "The gravitational potential and its derivatives for the prism". J Geod 76(8):475, DOI: 10.1007/s00190-002-0264-7

Novák P, Grafarend EW (2005) Ellipsoidal representation of the topographical potential and its vertical gradient. J Geod 78(11–12):691–706, DOI: 10.1007/s00190-005-0435-4

Novák P, Vaníček P, Martinec Z, Véronneau M (2001) Effects of the spherical terrain on gravity and the geoid. J Geod 75(9–10):491–504, DOI: 10.1007/s001900100201

Nowell DAG (1999) Gravity terrain corrections – an overview. J Appl Geophys 42:117–134

Papp G, Wang ZT (1996) Truncation effects in using spherical harmonic expansions for forward local gravity field modelling. Acta Geod Geoph Hung 31(1–2):47–66

Paul MK (1974) The gravity effect of a homogeneous polyhedron for three-dimensional interpretation. Pure Appl Geophys 112:553–561

Petrović S (1996) Determination of the potential of homogeneous polyhedral bodies using line integrals. J Geod 71(1):44–52, DOI: 10.1007/s001900050074

Rodriguez E, Morris CS, Belz JE, Chapin EC, Martin JM, Daffer W, Hensley S (2005) An assessment of the SRTM topographic products. Technical Report JPL D-31639, Jet Propulsion Laboratory, Pasadena, 143 pp

Schwarz K-P, Sideris MG, Forsberg R (1990) The use of FFT techniques in physical geodesy. Geophys J Int 100:485–514

Seitz K, Heck B (2001) Tesseroids for the calculation of topographic reductions. Abstracts "Vistas for Geodesy in the New Millenium", IAG 2001 Scientific Assembly 2–7 September 2001, Budapest, Hungary, 106

Sideris MG (1985) A fast Fourier transform method for computing terrain corrections. Manuscr Geod 10:66–73

Smith DA (2000) The gravitational attraction of any polygonally shaped vertical prism with inclined top and bottom faces. J Geod 74(5): 414–420, DOI: 10.1007/s001900000102

Smith DA (2002) Computing components of the gravity field induced by distant topographic masses and condensed masses over the entire Earth using the 1-D FFT approach. J Geod 76(3):150–168, DOI: 10.1007/s00190-001-0227-4

Smith DA, Robertson DS, Milbert DG (2001) Gravitational attraction of local crustal masses in spherical coordinates. J Geod 74(11–12):783–795, DOI: 10.1007/s001900000142

Talwani M, Ewing M (1960) Rapid computation of gravitational attraction of three-dimensional bodies of arbitrary shape. Geophysics 25:203–225

Tsoulis D (1999) Analytical and numerical methods in gravity field modelling of ideal and real masses. Reihe C, Heft Nr 510, Deutsche Geodätische Kommission, München

Tsoulis D, Tziavos IN (2002) A comparison of some existing methods for the computation of terrain correction in local gravity field modelling. In: Tziavos IN (ed) Gravity and Geoid 2002. Proceedings of the 3rd meeting of the international gravity and geoid commission, Thessaloniki, pp 156–160

Tsoulis D, Wziontek H, Petrović S (2003) A bilinear approximation of the surface relief in terrain correction computations. J Geod 77(5–6):338–344, DOI: 10.1007/s00190-003-0332-7

Vaníček P, Novák P, Martinec Z (2001) Geoid, topography, and the Bouguer plate or shell. J Geod 75(4):210–215, DOI: 10.1007/s001900100165

Vaníček P, Tenzer R, Sjöberg LE, Martinec Z, Featherstone WE (2004) New views of the spherical Bouguer gravity anomaly. Geophys J Int 159:460–472